HHS Public Access

Author manuscript

Nat Immunol. Author manuscript; available in PMC 2014 September 09.

Published in final edited form as:

Nat Immunol. 2013 September ; 14(9): 949–958. doi:10.1038/ni.2682.

Inflammation-induced effector CD4+ T cell interstitial migration is alpha-$_v$ integrin dependent

Michael G. Overstreet[*,^,6], **Alison Gaylo**[*,^], **Bastian Angermann**[2], **Angela Hughson**[*], **Young-min Hyun**[*], **Kris Lambert**[*], **Mridu Acharya**[3], **Alison C. Billroth-Maclurg**[*], **Alexander F. Rosenberg**[5], **David J. Topham**[*], **Hideo Yagita**[4], **Minsoo Kim**[*], **Adam Lacy-Hulbert**[3], **Martin Meier-Schellersheim**[2], and **Deborah J. Fowell**[*,1]

[*]David H. Smith Center for Vaccine Biology and Immunology, Aab Institute of Biomedical Sciences, Department of Microbiology and Immunology, University of Rochester, Rochester NY 14642, USA

[2]Computational Biology Unit, Laboratory of Systems Biology, National Institute of Allergy and Infectious Diseases, National Institutes of Health, Juntendo University, Tokyo, Japan

[3]Program of Developmental Immunology, Department of Pediatrics, Massachusetts General Hospital/Harvard Medical School, Juntendo University, Tokyo, Japan

[4]Department of Immunology, Juntendo University, Tokyo, Japan

[5]Division of Allergy, Immunology and Rheumatology, University of Rochester Medical Center, Rochester NY

Abstract

Leukocytes must traverse inflamed tissues to effectively control local infection. Although motility in dense tissues appears to be integrin-independent actin-myosin based, during inflammation changes to the extracellular matrix (ECM) may necessitate distinct motility requirements. Indeed, we found that T cell interstitial motility was critically dependent on RGD-binding integrins in the inflamed dermis. Inflammation-induced deposition of fibronectin was functionally linked to increased α_v integrin expression on effector CD4$^+$ T cells. Using intravital multi-photon imaging, we found that CD4$^+$ T cell motility was dependent on α_v expression. Selective α_v blockade or knockdown arrested T_H1 motility in the inflamed tissue and attenuated local effector function.

[1]Corresponding Author: Dr. Deborah J. Fowell, David H. Smith Center for Vaccine Biology and Immunology, University of Rochester, 601 Elmwood Avenue, Box 609, Rochester, NY 14642, Tel. 585-273-3680, FAX. 585-273-2452, Deborah_Fowell@urmc.rochester.edu.

[^]These authors contributed equally

[6]Current Address: Amplimmune, Inc. 45 West Watkins Mill Road, Gaithersburg, MD 20878

AUTHOR CONTRIBUTIONS

M.G.O, A.G. and D.J.F designed the study. M.G.O., A.G, K.L., M.A., A.B-M., A.H. and Y-M.H. performed the experiments. M.G.O., A.G. B.A., A.R., M.M-S and D.J.F analyzed the data. Y-M.H., M.K., D.J.T., A.L-H., H.Y., M.M-S provided reagents and conceptual advice. M.G.O. and D.J.F. wrote the manuscript.

COMPETING FINANCIAL INTERESTS

The authors declare no competing financial interests.

These data show a context-dependent specificity of lymphocyte movement in inflamed tissues that is essential for protective immunity.

Pathogen clearance requires effector T cells to migrate into inflamed tissues to locate the infected microenvironment. The molecular mechanisms involved in the migration of leukocytes into tissues via extravasation have been well characterized[1]. However, the interactions controlling movement through peripheral tissues are less well understood.

Integrins play a vital role in leukocyte trafficking from blood into tissues. Chemokine-mediated integrin activation leads to firm adhesion of leukocytes to the endothelium, essential for tranendothelial migration. In contrast, leukocyte interstitial migration is thought to be largely integrin-independent[2]. Migration studies using artificial collagen matrices or confinement chambers suggest that the dense three-dimensional ECM scaffold supports the use of non-adhesive, actin-based traction mechanisms by leukocytes[3, 4]. In the lymph node (LN), T cells migrate along networks of fibroblastic reticular cells (FRCs) that express integrin ligands ICAM-1 and VCAM-1 and chemokines CCL19 and CCL21. However, motility is driven by chemokine-mediated chemotaxis/haptotaxis directly and does not require integrins for adhesion[5]. Similarly, genetic ablation of all known integrins in DCs failed to perturb DC migration in the LN or skin[6]. Thus, under a variety of conditions, integrins appear to be largely dispensable for extravascular trafficking of leukocytes.

Inflammatory mediators and pathogens themselves modify ECM density and composition in peripheral tissues which may dictate new requirements for leukocyte motility at sites of inflammation[7]. T cells expressing distinct integrins accumulate in particular inflammatory settings and in discrete tissues where integrin expression is thought to play a role in tissue-specific homing[8] and retention within the tissue[9]. In contrast to the situation in LNs, where collagen fibers are coated by FRCs, T cells in non-lymphoid tissues such as the skin and lung are directly exposed to collagen fibers and associated ECM components that could act as guidance cues for movement through the interstitial space. The use of multiphoton microscopy has enabled the visualization of leukocyte motility within peripheral tissues with studies highlighting a close association between T cells and matrix fibers in skin, brain and tumors[10–16]. Lymphocyte movement in the skin during delayed type hypersensitivity showed a correlation between collagen-binding integrins on T cells and their migration along fibers requiring calcium signaling by Kv1.3 potassium-channels[14]. During infection with Toxoplasma in the brain, effector T cells also migrate along reticular fibers, although the brain was largely devoid of infection-induced increases in collagen[13]. In many studies, blockade of G protein-coupled receptor signaling attenuated leukocyte interstitial motility, but it is not clear if this is due to blockade of chemotaxis/kinesis *per se* or the absence of chemokine-induced integrin activation. Although neutrophil interstitial migration in the mesentery was shown to be integrin dependent[17], there have been no studies that directly test the role of integrins in T cell motility within inflamed peripheral tissues.

Given the critical role that physical confinement plays in three-dimensional cell motility[4] and the extent of inflammation-driven ECM remodeling, we addressed mechanisms of interstitial motility of effector $CD4^+$ T lymphocytes in the inflamed dermis. Inflammation was associated with a reduction in the density of collagen fibers and with extensive

fibronectin deposition. Using intravital multiphoton microscopy (IV-MPM) we found that effector CD4$^+$ T cell movement within the inflamed dermis is integrin-dependent and the expression of α_v-integrins is essential for interstitial motility and pathogen clearance. Thus, movement through inflamed interstitial tissue requires the coordinate expression of specific integrins on effector T cells with ECM changes in the tissue.

Results

Inflammation-induced migration along ECM fibers

Analysis of T cell interstitial migration was performed in the inflamed and non-inflamed dermis using intravital multiphoton microscopy (IV-MPM). Dermal location was assessed using the second harmonic generation (SHG) to distinguish the collagen-rich dermis from collagen-replete epidermis and from blood vessels using intravenous Texas-red dextran (Fig 1a, b). Cells were tracked over time in three-dimensional space using semi-automated software. T cells in the non-inflamed dermis were identified by using CD4-Cre+ Stop-floxed YFP mice (*Gt(ROSA)26Sor$^{tm1(EYFP)Cos}$* mice) (86% αβ+ T cells, the majority being CD4$^+$ and Foxp3$^-$, Supplementary Figure 1). In the steady state non-inflamed dermis T cells were observed at low frequencies and were uniformly non-motile (Fig 1c). Average velocities for dermal CD4$^+$ T cells (predominantly αβ T cells) were 0.803 ± 0.05 SEM μm/min; noticeably less than that observe for actively surveying dermal γδ T cells in the steady state (average speeds of 2–5 μm/min)[18, 19]. For T cell migration in the inflamed dermis, we followed a population of antigen-specific CD4$^+$ T cells. Naïve CD4$^+$ T cells from WT15 T cell receptor (TCR)-transgenic mice[20] were primed *in vitro* under T_H1 differentiation conditions. Primed cells were labeled with CFSE and transferred into naïve BALB/c mice that were immunized in the ear dermis with cognate peptide emulsified in CFA. Kinetic analysis in the inflamed dermis defined the peak of effector T cell accumulation in the tissue to be 3–4 days after immunization (data not shown). Inflammation led to striking changes in dermal T cell velocities (Fig 1c, Supplementary movie 1), consistent with previous models[14, 21, 22]. The T cells exhibited no preferential directionality in their crawling patterns and the mean squared displacement (MSD) of their crawling tracks increased linearly over time, suggesting that these cells were not following a chemotactic gradient within the tissue (Fig 1d, e). T cells crawled preferentially in the lateral plane (XY) of this tissue, with limited vertical (Z-axis) translocation (Supplementary Fig 2). *In vivo*-primed effector cells were visualized using donor T cells from a YFP-IFN-γ reporter mouse[23] and revealed crawling velocities and patterns similar to the adoptive transfer of *in vitro*-primed effector T cells (Fig 1f, Supplementary Fig 3). Thus, inflammation drives the recruitment and interstitial motility of effector T cells in the dermis. This enhanced T cell motility in the presence of inflammation and/or microbial stimuli is in contrast to dermal dendritic cells that are motile in non-inflamed dermis but immobile when exposed to microbial stimuli[24] suggesting cell type-specific cues for motility and arrest.

Imaging revealed dramatic changes in the collagen fibers of the inflamed skin, as visualized by second harmonic generation (SHG) (Fig 2a). Compared to collagen structure in untreated skin, characterized by dense layers of interwoven collagen fibers, the collagen in CFA-inflamed skin was a loose network of thick collagen bundles (Fig 2a–c). The collagen fibers

were also preferentially oriented in the XY plane (Supplementary Fig 4). Many T cells appeared to be crawling in directional patterns that closely followed the local collagen fibers (Supplementary Fig 5, Supplementary movie 1). To test if there was preferential migration of T cells along the matrix scaffold, we developed an unbiased quantitative technique that utilized computational image analysis to compare frame-by-frame directional vectors of individual T cell migration patterns with the orientation of the matrix fibers (Fig 2d, e). Briefly, SHG images were translated into a map of discrete collagen fibers based on local SHG intensity gradients (Supplementary Fig 5, and On-line methods). We then compared the migratory directions of the T cells with directions of the "local" collagen fibers (those fibers within a 6 μm radius around the T cell centroid) (Fig 2f) and calculated the angle differences between the vectors representing the fibers and those representing the migrating cell (Fig 2g). If T cells preferentially moved parallel to the local ECM fibers, we would expect more observations in close alignment (small angle differences) between ECM fibers and T cell migration than if T cell migration was random. This was indeed the case (Fig 2h). We quantified the close alignment by calculating the fraction of observations with an angle difference smaller than 15° or 30° between fiber and migrating T cell (n=10 experiments). The fraction of closely aligned observations was significantly larger (p<0.0001) than would be expected from random T cell movement (Fig 2i). We conclude that T cells preferentially migrated in directions parallel to the local collagen structures, suggesting that T cells were utilizing a form of contact guidance. These data are consistent with a haptokinetic model of motility, in which cells migrate along a three-dimensional surface, interacting with bound ligand through cell-surface receptors.

Integrin-dependent motility in the inflamed dermis

The density of the matrix appears to be a key determinant of the mode of interstitial motility, with integrin-dependency increasing as the density of the matrix decreases[4]. Therefore, the inflammation-based changes in collagen density and the crawling pattern of T cells along the matrix fibers prompted us to revisit integrin-dependency for T cell interstitial migration. While imaging T cell migration in the dermis we administered a blocking antibody to β_1 integrin, a common receptor chain that pairs with various α-chains for binding to extracellular matrix components[25, 26]. Soon after i.v. injection of anti-β_1 all intradermal T cells stopped migrating (Fig 3a,b) and adopted a rounded morphology (Supplementary Fig 6, Supplementary movie 2), consistent with a loss of adhesion to the surrounding matrix. Blockade of LFA-1 (ICAM-binding) had no effect on interstitial motility (data not shown).

To confirm that β1 was necessary for motility in the inflamed skin, we analyzed T cells genetically deficient in the β_1-subunit, using OTII *itgb1*$^{flox/flox}$ *CD4*-Cre mice. β_1-deficient T cells displayed no functional defects in clonal expansion, cytokines, or tissue infiltration; as previously noted[27] (data not shown). However, in contrast to acute β_1 blockade, β_1-deficient T cells showed no defects in migration within the dermal interstitium (Fig 3c,d). The disconnect between acute blockade and genetic deficiency raised two possibilities: that antibody treatment leads to migratory arrest through activating T cell signaling or that there is genetic compensation. To test effects of anti-β_1 signaling independent of receptor-ligand blockade we treated effector T cells with antibody and monitored migration *in vitro* on β_2-dependent ICAM-1 and CXCL12 coated-plates (Supplementary Fig 7). Anti-β_1 treatment

did not lead to cell arrest, suggesting cross-linking β_1 is not sufficient to halt migration. To address redundancy/compensation, β_3 appeared to be the likely alternative matrix-binding integrin for lymphocytes. Indeed, anti-β_3 Ab treatment halted migration by β_1-deficient T cells in the inflamed dermis, showing β_3 can compensate in the genetic absence of β_1 (Fig 3e), but not during acute β_1-blockade (Fig 3a,b). Surprisingly, anti-β_3 treatment also led to acute migratory arrest of wild-type (WT) T cells (Fig 3f,g). Therefore, both β_1 and β_3 contribute to interstitial motility but neither is sufficient for full migration in WT T cells. Consistent with the ability of both β_1 and β_3 integrins to bind the RGD sequence found in many ECM components such as fibronectin, local administration of RGD peptides (but not control RAD peptides) led to striking T cell migratory arrest (Fig 3h–j, Supplementary movie 3). Thus, effector T cells require integrin-ECM interactions for T cell migration within the inflamed dermal interstitium.

Selective α_v-integrin dependency for dermal motility

β_1 and β_3 both pair with the α-subunit, α_v, prompting us to analyze effector T cell α-subunit usage in the inflamed dermis. We first monitored receptor expression on a synchronous cohort of effector T cells through the adoptive transfer of naïve WT15 cells followed by immunization with LACK-CFA (Fig 4a). Five days after cell transfer and immunization we observed a restricted pattern of integrin expression on the effector T cells in the inflamed dermis with effector T cells expressing α_2, α_4 and α_v subunits, but little α_1 and no α_5 (Fig 4a). To rigorously test the role of these individual α-subunits in T cell motility we used acute antibody blockade and IV-MPM imaging. We found a highly restricted requirement for α_v in effector T cell motility in the inflamed dermis (Fig 4b, c, Supplementary movie 4); blockade of α_1, α_2, α_1+α_2, or α_4 failed to arrest T cell motility. Thus, $\alpha_v\beta_1$ and $\alpha_v\beta_3$ appear to be uniquely required for T cell interstitial motility. The finding that T cells may use both $\alpha_v\beta_1$ and $\alpha_v\beta_3$ to migrate through the CFA-inflamed dermis suggests that α_v expression may be limiting: acute perturbations to either β-subunit reduces the surface pool of α_v-integrins below a threshold needed for migration.

Fibronectin is a primary substrate for α_v integrins[28]. However, dermal fibronectin is sparse in the steady state, non-inflamed tissue (Fig 4d[29, 30]). Analysis of CFA-inflamed tissue sections revealed widespread increases in dermal fibronectin throughout the tissue (Fig 4d), consistent with previous observations in humans and hamsters[29–31]. Co-staining for types I and III collagen showed that fibronectin was closely associated with the interstitial collagen fibers (Fig 4e and Supplementary Fig 8) as previously observed[32]. Thus, in the inflamed dermis, dramatic changes in the collagen density are accompanied by increases in tissue fibronectin, consistent with a role for the RGD-dependent α_v-integrin in T cell motility.

Coordinate expression of integrins and ECM

We next asked if expression of α_v was restricted to a particular inflammation or tissue type. Robust expression of α_v was seen in the dermis in numerous inflammatory settings including a Th2 model of atopic or allergic inflammation and infection with the protozoa *Leishmania major* (Fig 5a, b) in both C57BL/6 (T_H1-dominated) and BALB/c mice (Th2 dominated) (data not shown) and also acute barrier disruption from tape stripping (Fig 5b). Similarly, pathogen-induced inflammation in the lung (Influenza) and gut (*H. polygyrus*)

and autoimmune infiltrates in the diabetic pancreas all showed uniformly high expression of α_v on infiltrating CD4$^+$ T cells. Therefore, α_v expression on effector CD4$^+$ T cells is observed across tissues and inflammation types. To identify possible context-dependent changes in T cell integrin expression we examined other matrix-binding α-integrin subunits. Using an unbiased hierarchical clustering analysis of the frequency of integrin-expressing T cells, T cells clustered into two principal groups based on tissue type (Fig 5b). Expression of collagen-binding integrins, α_1 and α_2, were markedly different between tissues: α_2 but not α_1 was expressed on effector CD4$^+$ T cells in the skin under all inflammatory settings (Fig 5b) while effector T cells in the lung expressed high levels of both α_1 and α_2 (Fig 5c)[9, 33]. T cells from the autoimmune inflamed pancreas segregated away from T cells in strong microbial-induced inflammatory settings, expressing little α_1 or α_2.

To examine the relationship between T cell matrix-binding integrins and the type of ECM components, we compared two examples of differential integrin expression and evaluated collagen and fibronectin in the respective inflamed tissues (Fig 5d). As noted above, in the CFA/OVA inflamed dermis α_v was expressed by effector T cells and was critical for motility (Fig 4a–c) consistent with co-localization of fibronectin and collagen fibers (Fig 4e, 5d). Expression of α_2, but not α_1, correlated with inflammation-induced expression of collagens I and III (α_2 ligands) but not collagen IV (α_1 ligand) (Supplementary Fig 8). In contrast, in the influenza infected lung (day 8 post-infection) high α_1 and α_2 expression by effector T cells (Fig 5c) was associated with large areas of the lung parenchyma that were rich in collagen III but low in fibronectin (Fig 5d, left panels) with extensive collagen IV around blood vessels, airways and alveoli as described[33]. The collagen III rich areas were coincident with the leukocytic infiltrates (Fig 5d, DIC image) and were not seen in uninfected lungs (data not shown). Similarly, widespread T cell-collagen IV co-localization was previously seen around the airways[33]. Thus, the co-expression of both α_1 and α_2 and α_v integrins may facilitate migration through distinct collagen-rich and fibronectin-rich regions in the influenza-infected lung[33].

α_v-expression upregulated during T cell priming

α_v expression was consistently higher on T cells in the inflamed dermis compared to the LN (Fig 6a, Supplementary Fig 9). The regulation of matrix-binding integrins could occur directly in the inflamed tissue through local induction or selection of integrin-expressing effector T cells, or could be programmed during T cell activation in the LN, as seen for tissue-specific homing molecules[8, 34, 35]. To explore these possibilities, we examined the phenotype of activated T cells in the LN and in the inflamed tissue. Following intradermal immunization, LN antigen-specific T cells segregated into three distinct populations based on α_v and CD62L expression, with the majority of CD62L^{lo} cells expressing low levels of α_v (Fig 6a). In contrast, effector T cells that had migrated to the dermis were predominantly α_v^{hi}CD62L^{lo} (Fig 6a). Cells expressing the highest amounts of activation markers CD25 and glycosylated CD43 in the LN were preferentially α_v^{hi} CD62L^{lo} (Fig 6b). Blockade of LN egress using the S1P$_1$ receptor agonist, FTY720, led to a selective increase in the number of α_v^{hi}CD62L^{lo} cells in the LN and a reciprocal loss of α_v^{hi}CD62L^{lo} cells in the inflamed dermis (Fig 6c, d). Similar results were observed in a polyclonal CD4$^+$ T cell response to KLH/CFA and *Leishmania major* infection (Supplementary Fig 9). Thus effector CD4$^+$ T

cells destined to exit the LN and patrol peripheral tissues express high amounts of α_v integrin and low CD62L, consistent with "emigrant" effector T cells[36].

Essential role for α_v integrin in interstitial migration and effector function

As seen in β1-deleted T cells (Fig 3), T cells genetically deficient in α_v (OTII *itgav*$^{flox/flox}$ *CD4*-Cre+) remained motile in the inflamed dermis but were still susceptible to migratory arrest by RGD peptides (Fig 7a). Thus there appears to be a fundamental requirement for integrin-mediated motility in inflamed tissues as highlighted by the high degree of compensation following genetic ablation. To directly test the requirement for α_v in interstitial migration we turned to acute gene knock down using α_v-specific shRNA. β_1-deficient OT-II T cells (whose motility remains α_v-dependent, Fig 7b) were retrovirally-transduced with a control vector or an α_v-specific shRNA (Fig 7c) and transferred into C57BL/6 congenic mice for imaging. Testing two shRNA constructs, α_v-9 and α_v-10, (see Supplementary Fig 10 for α_v-10 data) we found that knockdown of α_v did not hinder effector T cell recruitment to the inflamed dermis (Fig 7d) or change T cell location within the tissue as both α_v-sufficient and α_v-deficient effector T cells could be found in the same dermal regions (Fig 7e). However, the stable loss of α_v (Fig 7c, f) significantly impaired the motility of the interstitial T cells (Fig 7g, h, Supplementary Fig 10, Supplementary movie 5). These data are especially remarkable because surface expression of α_v was only reduced by ~60% (Fig 7c, f), indicating that only a fraction of the α_v surface receptors need to be compromised to alter migration, thus pointing to an essential role for α_v integrins in T cells interstitial migration within the inflamed dermis.

To determine the functional significance of α_v expression we used both gene knockdown and antibody blockade approaches. OVA-specific β1-deficient effector T_H1 cells were transduced with control or α_v-9 shRNA expressing retrovirus and transferred to C57BL/6 congenic mice immunized with OVA/CFA. Both control vector and α_v-9 shRNA GFP+ expressing T cells homed to the inflamed dermis with similar frequency (Fig 7i) and number (Fig 7d). To determine 'in vivo' function, cells were harvested from tissues in buffers containing Brefeldin-A to block cytokine secretion and intracellularly stained for IFN-γ, without additional *in vitro* stimulation[37, 38]. Knockdown of α_v had no effect on the frequency of *ex vivo* IFN-γ-producers in the dLN (mean: 3,500 GFP+ IFN-γ producers, control vector; 3,540 GFP+ IFNγ producers, α_v-9 shRNA) highlighting α_v-deleted T cells are competent to make IFN-γ. Nonetheless, a reduction in T cell α_v expression led to a marked reduction in the frequency of IFN-γ-producers in the inflamed dermal tissue (Fig 7i). Thus, T cell interstitial motility is dependent on α_v and disruption of interstitial motility limits T cell effector function, as represented here by IFN-γ production, presumably by limiting their ability to encounter antigen-bearing APCs in the inflamed tissue. Clearance of the protozoa *L. major* is critically dependent on IFN-γ-production by $CD4^+$ T cells localized to the infected dermis. Therefore, to test if the reduction in IFN-γ production might impact on pathogen clearance, we infected WT mice with the protozoa *L. major* and administered blocking anti-α_v antibody. Anti-α_v or control antibody was administered 4 weeks after *L. major* infection, for a 3 week period, when the C57BL/6 mice are mounting a protective IFN-γ-dependent anti-parasite immune response. As with shRNA knock-down, antibody blockade of α_v did not limit the generation of anti-*Leishmania* T cells in the LN (similar

IL-4/IFNγ ratio in all C57BL/6 groups, data not shown) or limit the number of $CD4^+$ T cells and macrophages that accumulated at the infection site (Fig 7j). However, blocking α_v had a significant impact on the ability to clear the pathogen (Fig 7k); with α_v blockade leading to significantly higher parasite titers. Attenuated pathogen clearance is consistent with the reduced ability of T cells to mount an efficient IFN-γ–response. However, we cannot exclude alternative mechanisms such as an effect of α_v-blockade on macrophage localization or function. Our studies find that integrin-dependent interstitial motility is essential for efficient IFN-γ effector T cell function in inflamed tissues and contributes, in part, to pathogen clearance.

DISCUSSION

Here we identify α_v (with β_1 or β_3) as a key receptor for intradermal motility of effector $CD4^+$ T cells. Integrin-dependency in interstitial motility of leukocytes has been controversial with previous studies supporting a largely integrin-independent mode of migration[5,6]. However, more recent studies suggest migration modes appear to be highly dynamic, with dendritic cells seamlessly moving between integrin-dependent and integrin-independent motility[39, 40]. Thus the requirement for integrin-driven motility is likely to be context-dependent and influenced by inflammation-induced changes in the tissue microenvironment. We found that T cells are essentially non-motile in non-inflamed tissue but motility is dramatically enhanced during inflammation in a manner dependent on integrins $\alpha_v\beta_1$ and/or $\alpha_v\beta_3$. In the CFA-inflamed dermis, significant structural changes in the density and composition of the tissue extracellular matrix occur, which may create an environment where lymphocytes are dependent on integrins for motility. Integrin specificity appears to be coordinately regulated with the type of ECM changes in the inflamed tissue. Fibronectin has long been known to bind to collagen and serve as a cell adhesion substrate[32] and we speculate that the inflammation-driven increase in fibronectin of the dermal interstitium observed across species[29–31] provides a substrate for infiltrating lymphocytes. Intriguingly, T_H1 effector cells are unique among leukocytes in their ability to synthesize fibronectin[41] possibly suggesting an active role for effector T cells in contributing to substrate deposition to facilitate interstitial migration. Our data show that the upregulation of α_v can be initiated during T cell activation in the LN, although further selection or regulation of integrin-expressing cells may occur locally as the effector T cells enter the inflamed microenvironment. Using IV-MPM, we found that the expression of α_v is critical for the rapid amoeboid movement of effector T cells in the inflamed dermis and that perturbation of α_v limits T cell effector function and attenuates efficient *L. major* clearance.

Chemokines direct tissue-specific homing and localization within tissues and are critical for the activation of leukocyte integrins (LFA-1, Mac-1) for firm adhesion during transendothelial migration (TEM). Although not directly tested here, we speculate that the integrin-dependent interstitial movement in the dermis is also contingent on chemokines for integrin activation. Indeed, many studies show a requirement for pertussis toxin-sensitive G-protein coupled receptors for interstitial motility. Lymphocyte crawling during TEM occurs via the dynamic assembly-disassembly of high affinity LFA-1 in adhesive filopodia and is essential for crawling under shear flow[42, 43]. Future studies with fluorescently-tagged α_v should reveal the dynamics of α_v expression in migrating T cells in inflamed tissues. During

TEM, shear forces promote migration through increases in invasive filopodia and accelerated dissociation of LFA-1:ICAM-1 interactions[42]. The edema associated with inflammation in tissues may also elevate 'interstitial' shear forces to promote integrin-dependent motility[44]. It is also possible that integrin activation could be regulated independently of chemokines, perhaps via CD44 as observed for TEM. Alternatively, it is possible that the integrin dependency underlies a need to adhere to ECM fibers to come into contact with immobilized chemokines rather than direct integrin-driven motility: disrupting integrin adhesion to ECM fibers could lead to an inability of cells to follow haptotactic gradients imposed by chemokines coating the fibers.

Integrins play a variety of roles in the immune response including promoting stable T cell-DC interactions for effector function, extravasation and tissue retention or survival. Distinct integrins direct tissue-specific homing ($\alpha_4\beta_7$ integrin and gut accumulation) and may determine location within the tissue as suggested by T cell α_1-integrin expression and their accumulation in the epidermis in the lung and skin[33,45]. Our data highlight an essential role for integrins in T cell movement through the inflamed tissue and suggest specific integrin expression is dictated by the changes in ECM components. As concluded from *in vitro* models[2], the density of the ECM scaffold may also influence the mode of motility with the degree of confinement dictating the utility of non-adhesive actin-myosin-based movement versus adhesive integrin-based migration[4]. Thus the mode of motility at sites of inflammation may differ depending on the extent of ECM remodeling, density or composition.

Interestingly, α_v itself plays a critical role in shaping the inflammatory microenvironment through modulating cytokine and matrix expression. α_v-binding to latent TGF-β via its RGD motif leads to TGF-β release from the ECM and biological activation[46] important in wound healing and fibrotic events. α_v also modulates induction of T_H17 and Treg differentiation via changes in dendritic cell function[47–49]. More recently the IL-4 and IL-13-induced matricellular protein, periostin[50], binds α_v integrin on keratinocytes to induce proinflammatory cytokines. Blockade of either periostin or α_v potently suppressed the allergic skin inflammation. Indeed, blockade or genetic ablation of α_v (mainly in myeloid cells) can inhibit inflammation in EAE, allergic asthma and lung scleroderma[47, 48, 51] although it precipitates ulcerative colitis[52]. The requirement for α_v for effector T cell interstitial migration through such inflamed sites may compound the therapeutic effects of targeting the α_v pathway in inflammation. Interestingly, this α_v-based motility is not required for gain of effector function or localization to the dermis but does limit robust execution of effector function, suggesting attenuation of interstitial migration limits the ability of effector T cells to scan the microenvironment of the inflamed tissue in search of specific antigen-bearing APCs.

Acute disruption of α_v via antibody blockade or shRNA knockdown revealed functional requirements for α_v in T cell interstitial motility. However, these were not recapitulated by genetic ablation experiments, with α_v-deficient T cells remaining highly motile through a compensatory mechanism dependent on RGD-binding integrins or other RGD-binding proteins. A similarly high degree of functional compensation for fibronectin-binding integrin subunits in knockout mice has been reported for developmental roles of α_v and α_5[53, 54] and

also for β_1 and β_3 in knockout cell lines[55]. These data therefore suggest a fundamental requirement for integrin-fibronectin (or other RGD-containing matrix proteins) interactions during both development and immune cell migration during inflammation.

Here we have show that inflammation in the dermis necessitates an integrin-based mechanism for effector T cell interstitial migration that is critical for full effector T cell function in the inflamed and infected tissue. As an intriguing perspective, it may be possible to predict the integrin requirements for interstitial migration in a given inflamed tissue by identifying the specific changes to the ECM landscape. Understanding the coordinate expression of leukocyte integrins and ECM substrates within inflamed tissues should provide novel therapeutic strategies for inflammation-specific and/or tissue-specific mitigation of immune-mediated tissue damage in autoimmunity and chronically inflamed pathologies.

On-line METHODS

Mice, Immunizations, and Infections

BALB/c and C57BL/6 mice were purchased from National Cancer Institute. LACK-specific TCR-Tg WT15 mice and IFN-γ reporter (Yeti) mice were provided by Drs. Nigel Killeen and Richard Locksley, respectively. CD11c-YFP mice were provided by Dr. Michel Nussenzweig. *itgb1*$^{fl/fl}$ mice. Albino B6 mice and *Gt(ROSA)26Sor*$^{tm1(EYFP)Cos}$ mice were purchased from Jackson Laboratories and CD4-Cre mice from Taconic Farms. itga5$^{fl/fl}$ mice provided by Dr. Richard Hynes. itgav$^{fl/fl}$ mice were provided by Dr Adam Lacy-Hulbert. Mice were bred and maintained in the pathogen-free animal facility at the University of Rochester. All animal procedures were approved by the Institutional Animal Care and Use Committee of the University of Rochester. Mice were immunized intradermally in the ear with 1 μg pLACK, 1 μg pOVA, or 5 ug Keyhole Limpit Hemacyanin (KLH) emulsified in Complete Freund's Adjuvant (CFA). For *Leishmania major* infection, mice were infected subcutaneously in the ear with 2×10^5 infectious parasites/ear. For Influenza infection, C57BL/6 mice were sedated with avertin and given a 30 uL intranasal inoculation of Influenza A/HK/X31 (9.2×10^7 PFU/ml). Eight days after infection, lungs were perfused and airway-resident cells were removed by bronchoalveolar lavage. Lymphocytes were then isolated from the lung tissue by collagenase digestion and Ficoll separation of viable cells. For *H. polygrus* infection, C57BL/6 mice were infected by gavage with 200 L3 *Heligmosomoides polygyrus* larvae. Ten days later, lamina propria lymphocytes were extracted from the small intestines using collagenase and a Percoll gradient after removal of Peyer's Patches. For tape-stripping, the ventral skin of the ear was tape stripped 10× by applying and gently removing adhesive tape (Scotch brand 610) followed by the application of 50μg OVA protein in 10uL PBS directly onto the stripped ear surface. Ears were harvested 5 days after tape stripping. For chronic allergic dermal sensitization, the ears were tape stripped three times, spaced three weeks apart. Samples were collected 48 hours after the final tape stripping and application of OVA. For the pancreas, diabetic NOD mice were identified when blood glucose levels exceeded 300mg/dl (usually 10–12 weeks of age). Young (6 weeks) non-diabetic mice were used as controls. Cells were isolated from the pancreas following collagenase digestion as for the ear dermis.

Antibodies and Reagents

All conjugated antibodies were purchased from eBioscience or Biolegend unless otherwise noted. For integrin expression on transferred WT15 T cells in the dermis, leukocytes were extracted from the ear and stained with CD45-Pacific Blue, CD4-AlexaFluor700, Thy-1.1-FITC and antibodies against one of the following: β_1-PE (Hmβ1-1), α_1-Alexa 488 or α_2-FITC (Ha31/8 and Ha1/29, respectively), α_3-APC (polyclonal, R&D Systems), α_4-PE (R1-2), purified α_5 (5H10-27), α_6-APC (GoH3) and α_v-PE (Hmα5-1 or RMV-7). Note that the anti-α_v specificity of the commercially available Hmα5-1 antibody clone (Biolegend) is different from that of the originally-described anti-α_5 clone (see supplementary Fig 10). Hmα5-1 binds to $CD4^+$ T cells from $itga5^{fl/fl}$ CD4-Cre+ mice but not $itgav^{fl/fl}$ CD4-Cre+ mice (Fig 13a) and precipitates α_v but not α_5 from activated T cell lysates (Fig 13b). Moreover, the Biolegend Hmα5-1 clone competes for binding with commercially available anti-α_v clone, RMV-7 (Supplementary Fig 10). Expression of α_5 on in vitro activated $CD4^+$ T cells was used to determine the specificity of Biolegend Hmα5-1 clone as expression of α_5 could not be detected on T cells activated in vivo (Supplementary Fig 10) under the variety of stimulatory conditions outlined in Fig 5. Of note, the absence of α_5 staining in vivo was not due to an α_5-specific sensitivity to enzymatic tissue digestion as positive α_5 staining on CD11b+ myeloid cells remained intact with/without enzymatic digestion (data not shown). Supplementary figure 10 directly compares the α_5-integrin specificity of the Biolegend Hmα5-1 clone and the original anti-α_5 clone from Yagita. For blocking *in vivo*, the following azide-free low endotoxin antibodies were injected through a tail vein catheter: anti-β1 (Hmβ1-1, eBioscience), anti-α_1 (Ha31/8), anti-α_2(Ha1/29), anti-α_4 (R1-2, Biolegend), anti-α_v (HMα5-1, Biolegend), anti-α_L (M17/4), and control Armenian Hamster IgG (H4/8). For FACS, cells were analyzed on an LSR II or a FACSCalibur (BD Biosciences, San Jose, CA). Data analyzed using FlowJo software (TreeStar).

Cell Culture and Adoptive Transfers

For *in vitro* T_H1 priming, $CD4^+$ cells were enriched from lymph node and spleen from WT15 Tg mice by complement-mediated lysis of $CD8^+$ (3.155), $CD24^+$ (J11D), and MHC-II^+ (M5/114) cells. Naïve T cells were then enriched by positive selection for $CD62L^+$ cells using a MACS column (Miltenyi Biotec): routinely >85% $CD4^+$ and >95% $CD62L^+$. Naïve T cells were stimulated with peptide-pulsed irradiated T cell-depleted splenocytes, IL-2 (10 U/mL), IL-12 (20 ng/mL), and anti-IL-4 (11B11, 40 μg/mL). Cells were split three days later and harvested on day five. The effector T_H1 cells were labeled with CFSE (Invitrogen, Carlsbad, CA) and transferred into mice (5×10^6 cells per mouse) prior to immunization. For WT15-Yeti cells, naïve $CD4^+$ T cells were enriched as described above and transferred directly into BALB/c mice without *in vitro* stimulation or labeling. The following day, mice were immunized with 5 μg pLACK/CFA in the ear dermis.

Extraction of T cells from the ear dermis

Ear tissue was processed as previously described[33]. Ears were excised, ventral and dorsal sheets separated and placed in collagenase D (1 mg/ml in PBS with 3mM $CaCl_2$, Roche) and incubated for 30 minutes at 37°C. EDTA was added (5mM) and the digested tissue disrupted using a pestle and metal strainer. Insoluble material was removed by filtration and

the pellet was washed twice in HBSS with 5% FCS. For ex vivo intracellular cytokine staining, Brefeldin A (1μg/ml) was added to all extraction and wash buffers to block cytokine secretion.

Intravital Multiphoton Microscopy and Image Analysis

Mice were anesthetized with isoflurane (induction ~5%, maintenance ~1.5%) (isoflurane vaporizer/ventilation machine, Lei Medical M3000R, VAP2100). Once anesthetized, a venous catheter was inserted in the lateral tail vein and the ventral side of the ear pinna was affixed to a coverslip. Mice were placed on a custom-made platform for imaging. Body temperature was maintained using a heated water pad and a heating block, monitored with a rectal thermometer. The microscope objective was heated (Bioptechs) to maintain normal dermal temperature during imaging. Images were acquired using an Olympus FV1000-AOM multiphoton system. Fluorescence was collected using an Olympus XLPlanN 25× NA1.05 objective for deep tissue multiphoton imaging and detected using two proprietary external photomultipliers (Hamamatsu, Japan). Fluorescence excitation was achieved by a Spectra-Physics DeepSee-MaiTai HP Ti:Sa laser tuned to 900 nm for excitation of CFSE and Texas Red. CFSE and Texas Red fluorescence was collected using 519/26nm and 607/36nm bandpass filters (Olympus and Semrock, respectively). YFP fluorescence was collected using 535/30nm bandpass filter (Chroma). Second harmonic signals were collected using a 447/60nm bandpass filter (Semrock). Z-stack images (512×512 pixels) were acquired with a vertical resolution of 3–5 μm and a lateral pixel size of 994nm. For time series, three-dimensional stacks were acquired every 40–45 seconds with a Kalman filter.

Raw imaging data were processed with Volocity software (Perkin Elmer) and ImageJ. A median filter was used to reduce noise and T cells were tracked using automated algorithms with manuals corrections. Raw tracking data was exported and processed in Excel. Cell tracks lasting for less than eight minutes were excluded from analyses. No minimum cell displacement criteria were imposed that would have excluded non-motile cells. Movies were created using both Volocity and ImageJ. For analysis of the effects of blocking antibodies, images were acquired for 20 minutes prior to treatment, followed by 25 minutes following treatment.

For quantitative analysis of collagen density, SHG images were obtained from the dermis of anesthetized mice that had been immunized three days previously in one ear with KLH/CFA. Control images were taken from the contralateral ear. Images stacks were taken at 512×512 resolution (994 nm/pixel) at 1 μm vertical intervals through the ear. Laser intensities and PMT voltages were adjusted with tissue depth to maintain visible SHG signal. Once acquired, 150×150 μm regions of the image stacks were selected to avoid hair follicles and major vasculature.

Analysis tool for migrating T cell—ECM association—ECM-fiber directions were estimated using ImageJ. The Differentials plug-in was used to calculate intensity gradients, which were rotated by 90 degrees and mapped to a range of [0..180] degrees to represent fiber directions. Our approach took advantage of the fact that the direction of strongest variation (intensity gradients) must be perpendicular to the fiber direction: any directions

pointing away from the fiber have a lower intensity than the directions that follow the fiber. We only determined lateral directions for this analysis (Fig 3a,b), since both T-cell movement and ECM-fiber direction are preferentially aligned in the X-Y plane (Supplementary Fig. 2,4,5). Cell locations were imported from tracking data and used to export fiber directions and gradient magnitudes from spheres with 6 μm radius around cell centroids. Extracted ECM-direction data and cell tracks were imported in R. Cell velocities were calculated using central differences and tracks with sedentary cells, which were defined as cells with a mean velocity of less than 2.5 μm/min were removed. For each observation of a cell in a track, we disregarded irrelevant direction samples stemming from background noise instead of ECM-fibers by considering only those samples that were in the 90^{th} percentile of the intensity gradient magnitude (Supplementary Fig 5). The local ECM-direction around the cell centroid was calculated as the gradient weighted mean of the selected direction samples.

FTY720 Treatment

Mice received FTY20 (1 mg/kg, Cayman Chemicals) i.p. 72 and 96 hours post-immunization. Control mice received vehicle alone.

RGD Peptide Treatment

BALB/c mice received CFSE-labeled effector T_H1 cells and were immunized as described above. Immediately prior to imaging, RGD or control RAD peptide was injected directly into the ear dermis (50 μg peptide, Peptides International).

Immunohistochemistry

Three days after immunization, ears were excised and frozen in OCT. Frozen sections were cut, fixed, and stained for ECM components. Primary antibodies against fibronectin (Abcam) and types I, III, and IV collagen (Southern Biotec) were used, followed by staining with Cy3- and AlexaFluor647-conjugated secondary antibodies (Jackson and Molecular Probes, respectively). For IHC analysis of influenza-infected lung tissue, lungs were excised eight days post-infection.

Retroviral Transduction

Naive $\beta1^{-/-}$ OT-II cells were purified from spleen and LN and stimulated with peptide/APC under T_H1 conditions. One day after the initiation of the culture, cells were transduced with MSCV encoding α_v shRNA or MSCV vector alone. Cells were then split on day 3 and harvested on day 5, similar to conditions with WT15 cells. On the day of harvest, transduction efficiency (indicated by % GFP+ cells) and α_v expression levels were measured by FACS. Transduction efficiencies were routinely between 15–30% and were similar between control vector and α_v shRNA MSCV.

Statistics

All statistical tests were done with GraphPad Prism or R software. Many analyses used the non-parametric Mann Whitney U test. For multiple analyses of variance, the Kruskal-Wallis

test was used with Dunn's post-test. For pairwise comparisons, Wilcoxon signed-rank test was used. ANOVA was used across multiple treatment groups.

Supplementary Material

Refer to Web version on PubMed Central for supplementary material.

ACKNOWLEDGEMENTS

The authors thank Ron Germain and Jackson Egen for technical assistance; Karl Kasischke, Linda Callahan, Ed Brown and the URMC Multiphoton Core for support; Beatriz Leon and Frances Lund for *H.polygyrus* infected tissue; Kihong Lim for technical assistance; Jim Miller and Steve Georas for comments on the manuscript; and members of the Fowell and Kim labs for discussion and support. This work was supported by National Institutes of Health grants AI072690 and AI088427 to D.J.F, HL018208 and HL087088 to M.K, AI089079 to M.G.O, and American Heart Association grant 11SDG7520018 to Y-M.H.

REFERENCES

1. Nourshargh S, Hordijk PL, Sixt M. Breaching multiple barriers: leukocyte motility through venular walls and the interstitium. Nat Rev Mol Cell Biol. 2010; 11:366–378. [PubMed: 20414258]
2. Friedl P, Weigelin B. Interstitial leukocyte migration and immune function. Nat Immunol. 2008; 9:960–969. [PubMed: 18711433]
3. Friedl P, Entschladen F, Conrad C, Niggemann B, Zanker KS. CD4+ T lymphocytes migrating in three-dimensional collagen lattices lack focal adhesions and utilize beta1 integrin-independent strategies for polarization, interaction with collagen fibers and locomotion. Eur J Immunol. 1998; 28:2331–2343. [PubMed: 9710211]
4. Jacobelli J, et al. Confinement-optimized three-dimensional T cell amoeboid motility is modulated via myosin IIA-regulated adhesions. Nat Immunol. 2010; 11:953–961. [PubMed: 20835229]
5. Woolf E, et al. Lymph node chemokines promote sustained T lymphocyte motility without triggering stable integrin adhesiveness in the absence of shear forces. Nat Immunol. 2007; 8:1076–1085. [PubMed: 17721537]
6. Lammermann T, et al. Rapid leukocyte migration by integrin-independent flowing and squeezing. Nature. 2008; 453:51–55. [PubMed: 18451854]
7. Sorokin L. The impact of the extracellular matrix on inflammation. Nat Rev Immunol. 2010; 10:712–723. [PubMed: 20865019]
8. Sigmundsdottir H, Butcher EC. Environmental cues, dendritic cells and the programming of tissue-selective lymphocyte trafficking. Nat Immunol. 2008; 9:981–987. [PubMed: 18711435]
9. Ray SJ, et al. The collagen binding alpha1beta1 integrin VLA-1 regulates CD8 T cell-mediated immune protection against heterologous influenza infection. Immunity. 2004; 20:167–179. [PubMed: 14975239]
10. Okada T. Two-photon microscopy analysis of leukocyte trafficking and motility. Semin Immunopathol. 2010; 32:215–225. [PubMed: 20603709]
11. Schumann K, et al. Immobilized chemokine fields and soluble chemokine gradients cooperatively shape migration patterns of dendritic cells. Immunity. 2010; 32:703–713. [PubMed: 20471289]
12. Bajenoff M, et al. Stromal cell networks regulate lymphocyte entry, migration, and territoriality in lymph nodes. Immunity. 2006; 25:989–1001. [PubMed: 17112751]
13. Wilson EH, et al. Behavior of parasite-specific effector CD8+ T cells in the brain and visualization of a kinesis-associated system of reticular fibers. Immunity. 2009; 30:300–311. [PubMed: 19167248]
14. Matheu MP, et al. Imaging of effector memory T cells during a delayed-type hypersensitivity reaction and suppression by Kv1.3 channel block. Immunity. 2008; 29:602–614. [PubMed: 18835197]

15. Boissonnas A, Fetler L, Zeelenberg IS, Hugues S, Amigorena S. In vivo imaging of cytotoxic T cell infiltration and elimination of a solid tumor. J Exp Med. 2007; 204:345–356. [PubMed: 17261634]
16. Mrass P, et al. Random migration precedes stable target cell interactions of tumor-infiltrating T cells. J Exp Med. 2006; 203:2749–2761. [PubMed: 17116735]
17. Werr J, Xie X, Hedqvist P, Ruoslahti E, Lindbom L. beta1 integrins are critically involved in neutrophil locomotion in extravascular tissue In vivo. J Exp Med. 1998; 187:2091–2096. [PubMed: 9625769]
18. Gray EE, Suzuki K, Cyster JG. Cutting edge: Identification of a motile IL-17-producing gammadelta T cell population in the dermis. J Immunol. 2011; 186:6091–6095. [PubMed: 21536803]
19. Sumaria N, et al. Cutaneous immunosurveillance by self-renewing dermal gammadelta T cells. J Exp Med. 2011; 208:505–518. [PubMed: 21339323]
20. Wang Q, et al. CD4 promotes breadth in the TCR repertoire. J Immunol. 2001; 167:4311–4320. [PubMed: 11591754]
21. Filipe-Santos O, et al. A dynamic map of antigen recognition by CD4 T cells at the site of Leishmania major infection. Cell Host Microbe. 2009; 6:23–33. [PubMed: 19616763]
22. Egawa G, et al. In vivo imaging of T-cell motility in the elicitation phase of contact hypersensitivity using two-photon microscopy. J Invest Dermatol. 2011; 131:977–979. [PubMed: 21248770]
23. Stetson DB, et al. Constitutive cytokine mRNAs mark natural killer (NK) and NK T cells poised for rapid effector function. J Exp Med. 2003; 198:1069–1076. [PubMed: 14530376]
24. Ng LG, et al. Migratory dermal dendritic cells act as rapid sensors of protozoan parasites. PLoS Pathog. 2008; 4:e1000222. [PubMed: 19043558]
25. Springer TA. Adhesion receptors of the immune system. Nature. 1990; 346:425–434. [PubMed: 1974032]
26. Campbell ID, Humphries MJ. Integrin structure, activation, and interactions. Cold Spring Harb Perspect Biol. 2011; 3
27. DeNucci CC, Shimizu Y. beta1 integrin is critical for the maintenance of antigen-specific CD4 T cells in the bone marrow but not long-term immunological memory. J Immunol. 2011; 186:4019–4026. [PubMed: 21357540]
28. Ruoslahti E. RGD and other recognition sequences for integrins. Annu Rev Cell Dev Biol. 1996; 12:697–715. [PubMed: 8970741]
29. Clark RA, Dvorak HF, Colvin RB. Fibronectin in delayed-type hypersensitivity skin reactions: associations with vessel permeability and endothelial cell activation. J Immunol. 1981; 126:787–793. [PubMed: 7005343]
30. Clark RA, et al. Fibronectin deposition in delayed-type hypersensitivity. Reactions of normals and a patient with afibrinogenemia. J Clin Invest. 1984; 74:1011–1016. [PubMed: 6381536]
31. Kusubata M, et al. Spatiotemporal changes of fibronectin, tenascin-C, fibulin-1, and fibulin-2 in the skin during the development of chronic contact dermatitis. J Invest Dermatol. 1999; 113:906–912. [PubMed: 10594729]
32. Klebe RJ. Isolation of a collagen-dependent cell attachment factor. Nature. 1974; 250:248–251. [PubMed: 4859375]
33. Richter M, et al. Collagen distribution and expression of collagen-binding alpha1beta1 (VLA-1) and alpha2beta1 (VLA-2) integrins on CD4 and CD8 T cells during influenza infection. J Immunol. 2007; 178:4506–4516. [PubMed: 17372009]
34. Campbell DJ, Butcher EC. Rapid acquisition of tissue-specific homing phenotypes by CD4(+) T cells activated in cutaneous or mucosal lymphoid tissues. J Exp Med. 2002; 195:135–141. [PubMed: 11781372]
35. Sigmundsdottir H, et al. DCs metabolize sunlight-induced vitamin D3 to 'program' T cell attraction to the epidermal chemokine CCL27. Nat Immunol. 2007; 8:285–293. [PubMed: 17259988]
36. Fazilleau N, McHeyzer-Williams LJ, Rosen H, McHeyzer-Williams MG. The function of follicular helper T cells is regulated by the strength of T cell antigen receptor binding. Nat Immunol. 2009; 10:375–384. [PubMed: 19252493]

37. McLachlan JB, Catron DM, Moon JJ, Jenkins MK. Dendritic cell antigen presentation drives simultaneous cytokine production by effector and regulatory T cells in inflamed skin. Immunity. 2009; 30:277–288. [PubMed: 19200757]
38. Sojka DK, Fowell DJ. Regulatory T cells inhibit acute IFN-gamma synthesis without blocking T-helper cell type 1 (Th1) differentiation via a compartmentalized requirement for IL-10. Proc Natl Acad Sci U S A. 2011; 108:18336–18341. [PubMed: 22025707]
39. Renkawitz J, et al. Adaptive force transmission in amoeboid cell migration. Nat Cell Biol. 2009; 11:1438–1443. [PubMed: 19915557]
40. Friedl P, Wolf K. Plasticity of cell migration: a multiscale tuning model. J Cell Biol. 2010; 188:11–19. [PubMed: 19951899]
41. Sandig H, et al. Fibronectin is a TH1-specific molecule in human subjects. J Allergy Clin Immunol. 2009; 124:528–535. 535 e521–525. [PubMed: 19541353]
42. Shulman Z, et al. Lymphocyte crawling and transendothelial migration require chemokine triggering of high-affinity LFA-1 integrin. Immunity. 2009; 30:384–396. [PubMed: 19268609]
43. Park EJ, et al. Distinct roles for LFA-1 affinity regulation during T-cell adhesion, diapedesis, and interstitial migration in lymph nodes. Blood. 2010; 115:1572–1581. [PubMed: 20023213]
44. Rutkowski JM, Swartz MA. A driving force for change: interstitial flow as a morphoregulator. Trends Cell Biol. 2007; 17:44–50. [PubMed: 17141502]
45. Conrad C, et al. Alpha1beta1 integrin is crucial for accumulation of epidermal T cells and the development of psoriasis. Nat Med. 2007; 13:836–842. [PubMed: 17603494]
46. Yang Z, et al. Absence of integrin-mediated TGFbeta1 activation in vivo recapitulates the phenotype of TGFbeta1-null mice. J Cell Biol. 2007; 176:787–793. [PubMed: 17353357]
47. Luzina IG, et al. Regulation of pulmonary inflammation and fibrosis through expression of integrins alphaVbeta3 and alphaVbeta5 on pulmonary T lymphocytes. Arthritis Rheum. 2009; 60:1530–1539. [PubMed: 19404954]
48. Acharya M, et al. alphav Integrin expression by DCs is required for Th17 cell differentiation and development of experimental autoimmune encephalomyelitis in mice. J Clin Invest. 2010; 120:4445–4452. [PubMed: 21099114]
49. Paidassi H, et al. Preferential expression of integrin alphavbeta8 promotes generation of regulatory T cells by mouse CD103+ dendritic cells. Gastroenterology. 2011; 141:1813–1820. [PubMed: 21745448]
50. Masuoka M, et al. Periostin promotes chronic allergic inflammation in response to Th2 cytokines. J Clin Invest. 2012; 122:2590–2600. [PubMed: 22684102]
51. Kudo M, et al. IL-17A produced by alphabeta T cells drives airway hyper-responsiveness in mice and enhances mouse and human airway smooth muscle contraction. Nat Med. 2012; 18:547–554. [PubMed: 22388091]
52. Lacy-Hulbert A, et al. Ulcerative colitis and autoimmunity induced by loss of myeloid alphav integrins. Proc Natl Acad Sci U S A. 2007; 104:15823–15828. [PubMed: 17895374]
53. Yang JT, Hynes RO. Fibronectin receptor functions in embryonic cells deficient in alpha 5 beta 1 integrin can be replaced by alpha V integrins. Mol Biol Cell. 1996; 7:1737–1748. [PubMed: 8930896]
54. van der Flier A, et al. Endothelial alpha5 and alphav integrins cooperate in remodeling of the vasculature during development. Development. 2010; 137:2439–2449. [PubMed: 20570943]
55. Wennerberg K, et al. Beta 1 integrin-dependent and -independent polymerization of fibronectin. J Cell Biol. 1996; 132:227–238. [PubMed: 8567726]

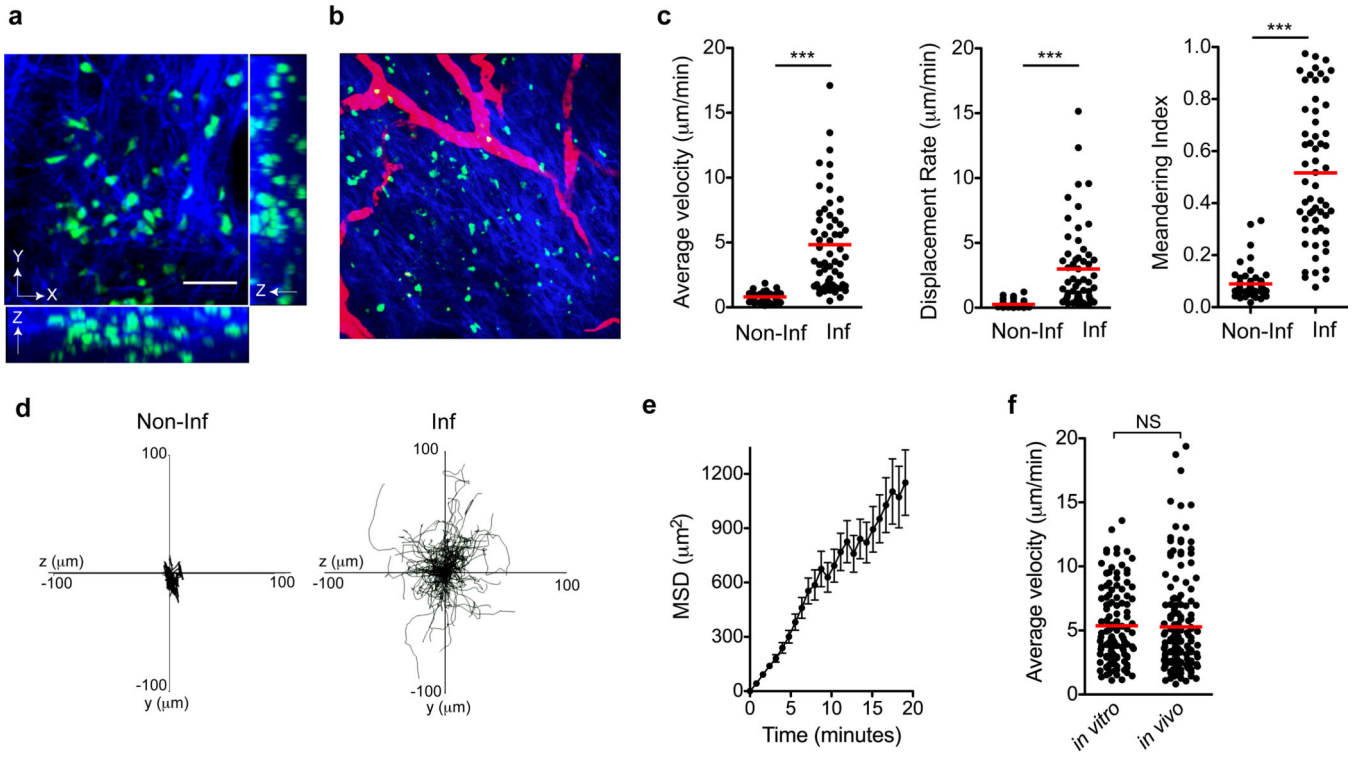

Figure 1. Migratory patterns of effector T_H1 T cells in the CFA-inflamed ear dermis

(a) Maximum intensity projections across X, Y, and Z axes of WT15 T cells (green) and collagen (second harmonic generation, blue) in the CFA-inflamed dermis. Scale bar, 40μm. **(b)** X-Y projection of T cells and SHG with vasculature shown in red using intravenous Texas Red-labeled dextran. **(c)** Steady-state (non-inflamed, Non-Inf) and CFA-inflamed (Inf) T cell motility by average velocity, displacement and meandering index. **(d)** X–Y projections of the T cell migration tracks over a 20-minute time span with CFA. **(e)** Mean squared displacement (MSD) of the T cell tracks show a linear increase over time. **(f)** Comparison of average velocities of T cells using adoptively transferred effector WT15 T cells (*in vitro*) or effector T cells primed *in vivo* using WT15 IFN-γ-YFP reporter cells to identify putative IFN-γ-producing cells (*in vivo*). Statistics by Mann-Whitney: ***$p<0.001$; NS, not significant, $p>0.05$. Data are representative of more than ten independent imaging experiments.

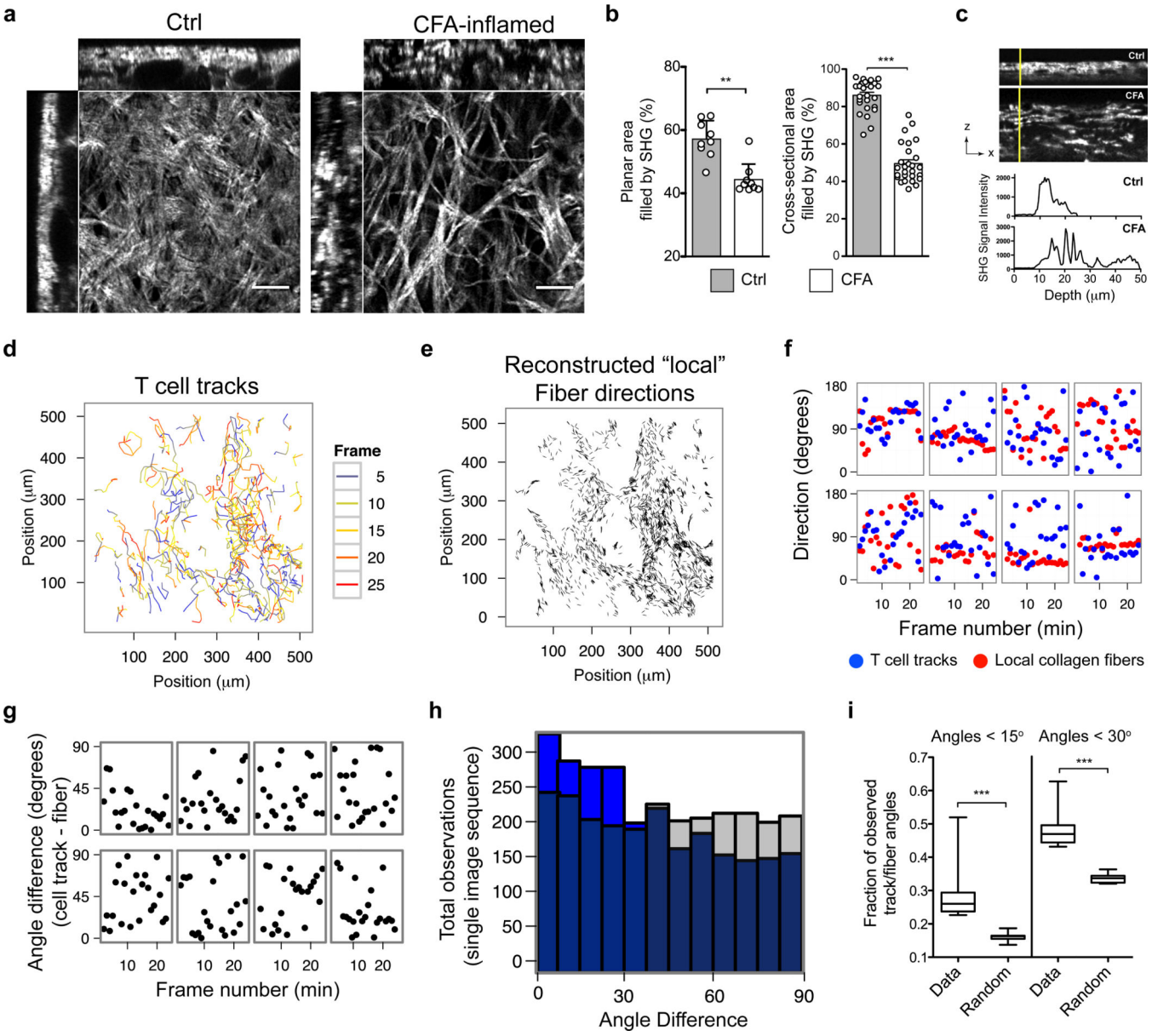

Figure 2. T cells migration is guided by ECM-fibers

BALB/c mice immunized with KLH/CFA in the ear dermis and analyzed by IV-MPM on day 3. Collagen structure by SHG. **(a)** Sample image volumes of non-immunized (Ctrl) and CFA-inflamed ears. **(b)** Analysis of planar area (XY) (left) and cross-sectional area (XZ) filled by SHG in control and CFA-inflamed ears. Left, each circle represents a unique region (150 μm × 150 μm area, avoiding hair follicles and blood vessels) from three different ears for each group. Right, each circle represents one of three orthogonal views analyzed for every one planar region analysis on the left. Bars represent mean ± SEM. **(c)** Cross-sectional images of SHG signal intensity in ear (top) and SHG across the vertical yellow lines (bottom). **(d)** Projection of cell tracks in x-y plane. Color code, frame at which T cell locations were observed. **(e)** Reconstructed fiber directions. **(f)** Migration and fiber directions along eight representative T-cell tracks. Directions are measured as angle relative

to the x-axis of the image data: blue dots, T cell tracks; red dots, fibers. **(g)** Angle differences between fiber and migration directions in **(f)**. **(h)** Histogram of angle differences for all tracks time steps from a single representative experiment (blue) compared to the distribution of angle differences that would result from random migration (grey). **(i)** Frequency of directional differences smaller than 15° and 30°, n=10 experiments. Statistical significances evaluated by Mann-Whitney: **p<0.01; ***p<0.001.

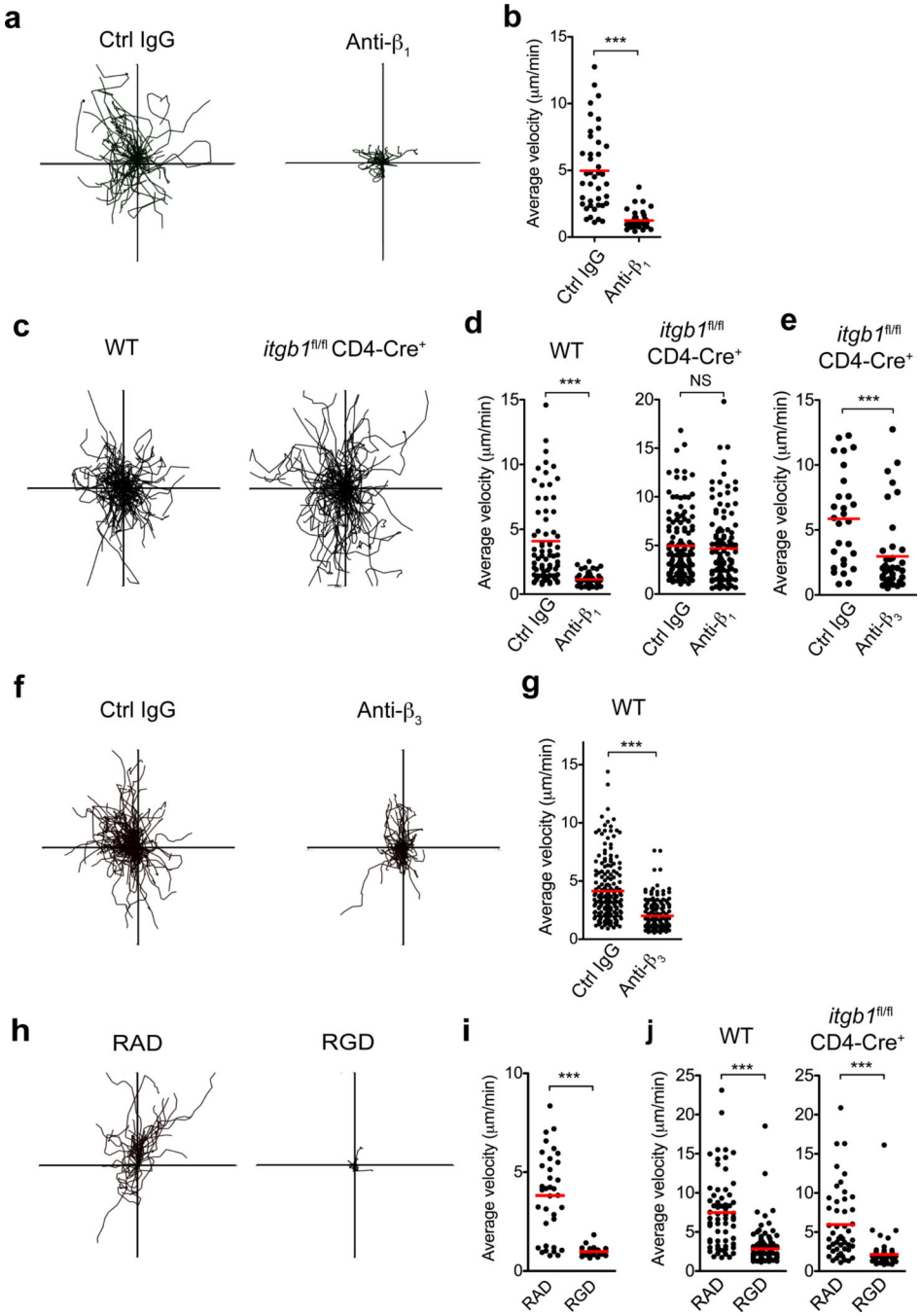

Figure 3. RGD-dependent integrin blockade impairs T cell motility in the inflamed dermis

(a, b) While imaging WT15 T cells in the inflamed ear dermis, control (Ctrl) IgG or a blocking antibody to β_1 integrin were administered intravenously. **(a)** XY projections of T cell migratory paths over 25 minutes immediately following control IgG or anti-β_1 integrin treatment (100 μg antibody). **(b)** Average velocity of T cells. **(c)** WT or β_1-deficient (*itgb1*$^{fl/fl}$ × CD4-Cre+) OT-II T cells were imaged in the dermis and the resultant T cell crawling patterns are shown. **(d)** Blocking antibodies to β_1 integrin were administered intravenously and OT-II T cell migration velocities shown for both WT and β_1-deficient

cells. **(e)** β_1-deficient T cell migration velocities after blocking antibodies to β_3 integrin. **(f–g)** While imaging WT OT-II T cells in the dermis, blocking antibodies to β_3 integrin were administered intravenously and the resultant T cell crawling patterns (**f**) and migration velocities (**g**) are shown. **(h–j)** Immediately prior to imaging of adoptively transferred WT effector WT15 T cells, control RAD or integrin-blocking RGD peptides were injected into the CFA-inflamed ear dermis. **(h)** XY projections of T cell migratory paths over 25 minutes. **(i)** Average velocity of T cells over the same time period. **(j)** Immediately prior to imaging of WT and β_1-deficient OT-II T cells in the inflamed dermis, control RAD or blocking RGD peptides were injected into the ear dermis and resultant T cell migration velocities are shown. Statistics by Mann-Whitney: ***$p<0.001$; NS, not significant, $p>0.05$.

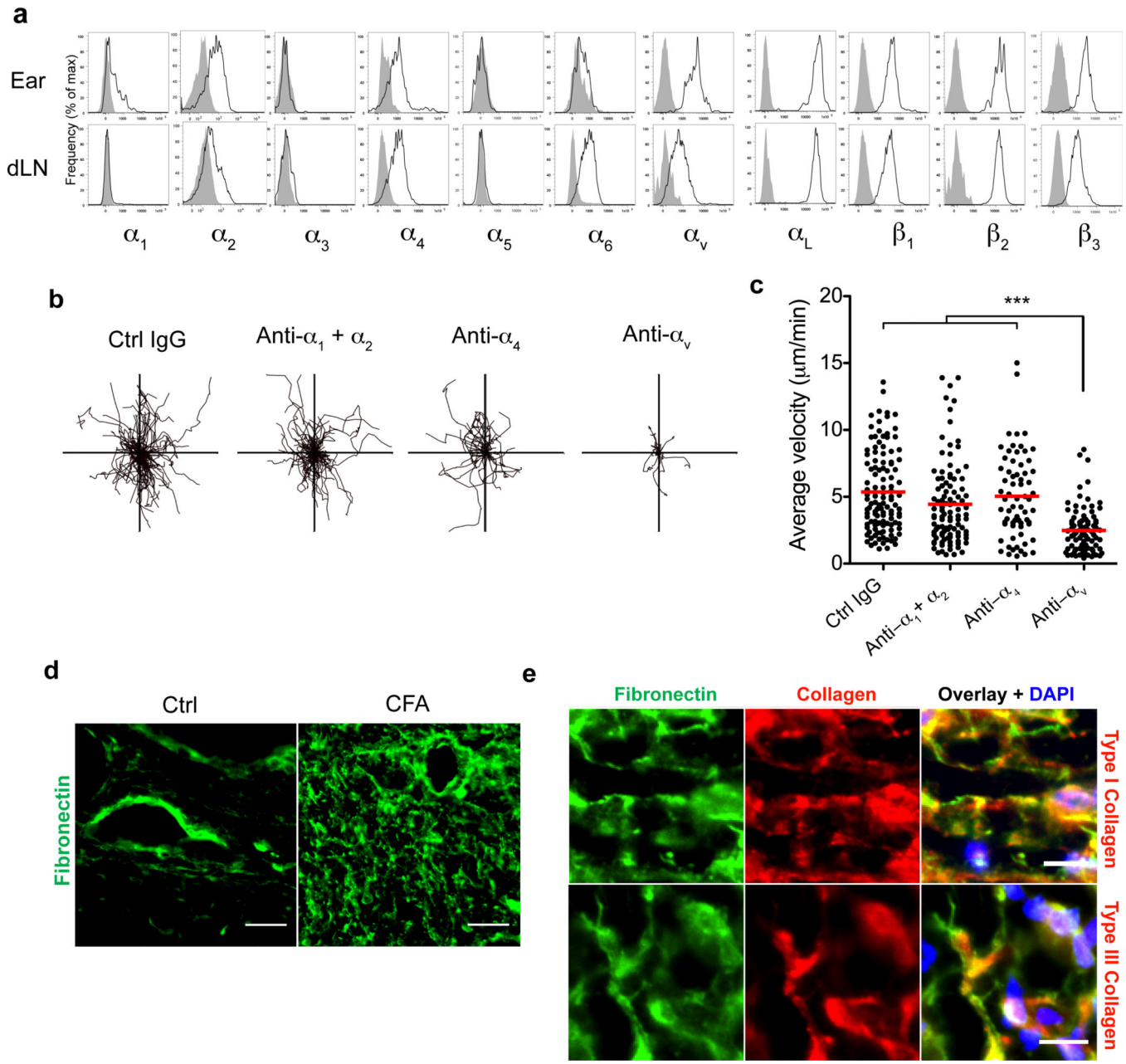

Figure 4. CD4$^+$ T cells utilize α_v integrin for intradermal motility

(a) Integrin expression by *in vivo*-primed WT15 cells in the immunized ear dermis and draining lymph node five days after immunization. Histograms represent viable donor CD4$^+$Thy-1.1$^+$ (WT15) lymphocytes: integrin staining (black line) and isotype control staining (grey shaded). **(b,c)** While imaging effector WT15 T cells in the inflamed ear dermis, control (Ctrl) IgG or blocking antibodies (100 μg each) to the indicated integrin subunits were administered intravenously. XY projections of T cell migratory paths over 25 minutes immediately following treatment with indicated blocking antibody. **c.** Average velocities of T cells over the same time periods and treatments. **(d)** Immunohistological staining of fibronectin on frozen sections of control (non-inflamed, Ctrl) and KLH/CFA-

immunized ears three days after immunization. Scale bar, 25μm. **(e)** Co-staining of fibronectin and types I or III collagen on KLH/CFA-inflamed ears. Scale bar, 10μm. Data are representative of at least three independent experiments for all antibody-blocking experiments. For **(c)** statistical significance was evaluated by a Kruskal-Wallis test with Dunn's post-test; *** $p<0.001$.

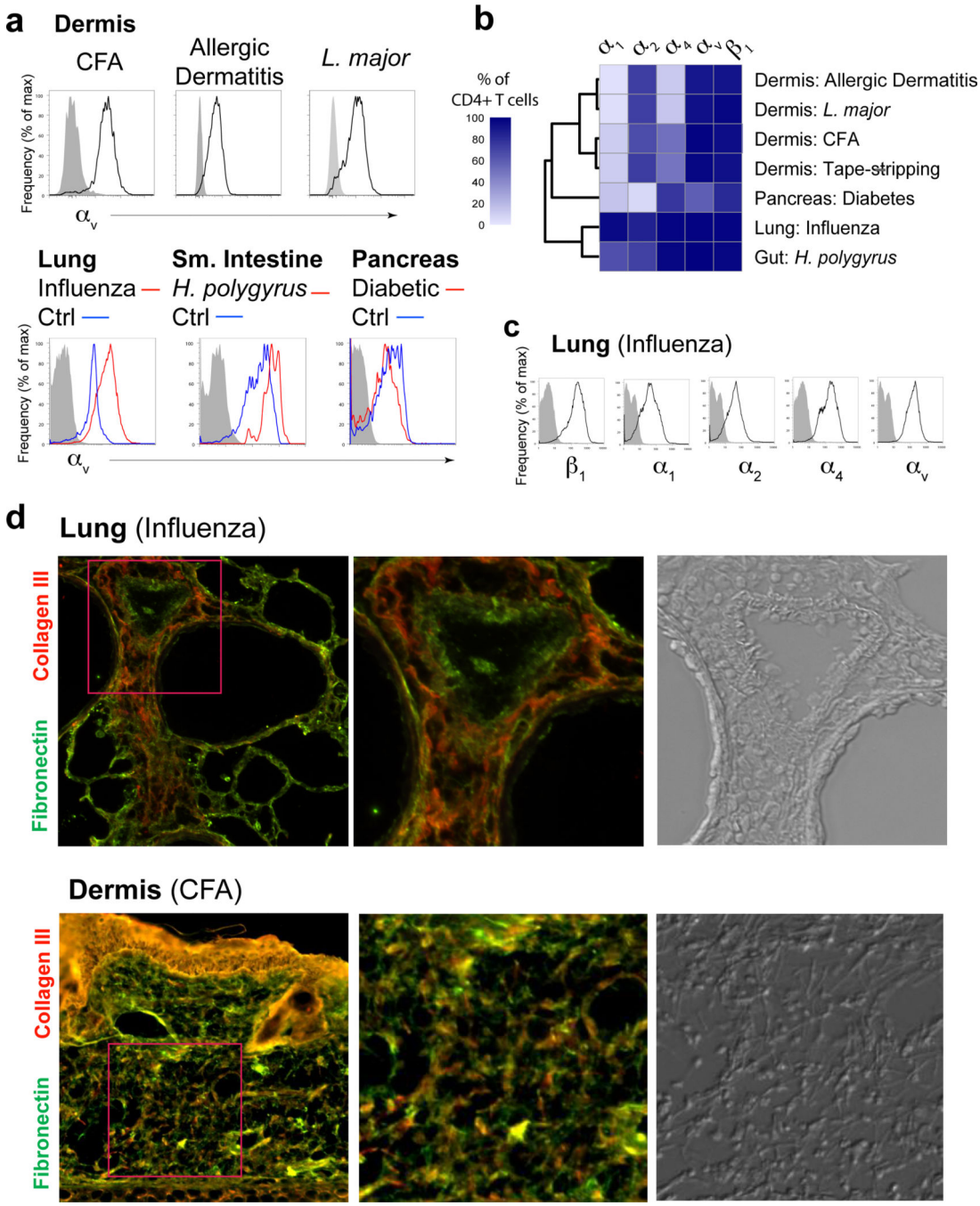

Figure 5. Broad α_v integrin expression by effector CD4$^+$ T cells across tissues and types of inflammation

(a) Histogram profiles of α_v integrin expression on total CD4$^+$ T cells extracted from the ear dermis (top) and other tissues (bottom). Where indicated, α_v expression on CD4$^+$ T cells from non-inflamed (control) tissues are shown (blue line), compared to inflamed/infected tissue (red line) and isotype control staining (grey shaded). **(b)** Hierarchical clustering of the frequency of integrin-expressing T cell populations from different tissues. **(c)** Histogram expression profiles of indicated alpha chain integrin subunits on CD4$^+$ T cells extracted

from influenza-infected lung tissue (day 8 post-infection) compared to isotype control staining (grey shaded). **(d)** Comparison of fibronectin and collagen immunohistochemistry on tissues from influenza-infected lung (day 8) (top row) and CFA-inflamed dermis (bottom row). Second panels are larger representations of boxed areas from first panel. Third panel is a DIC image of same boxed area.

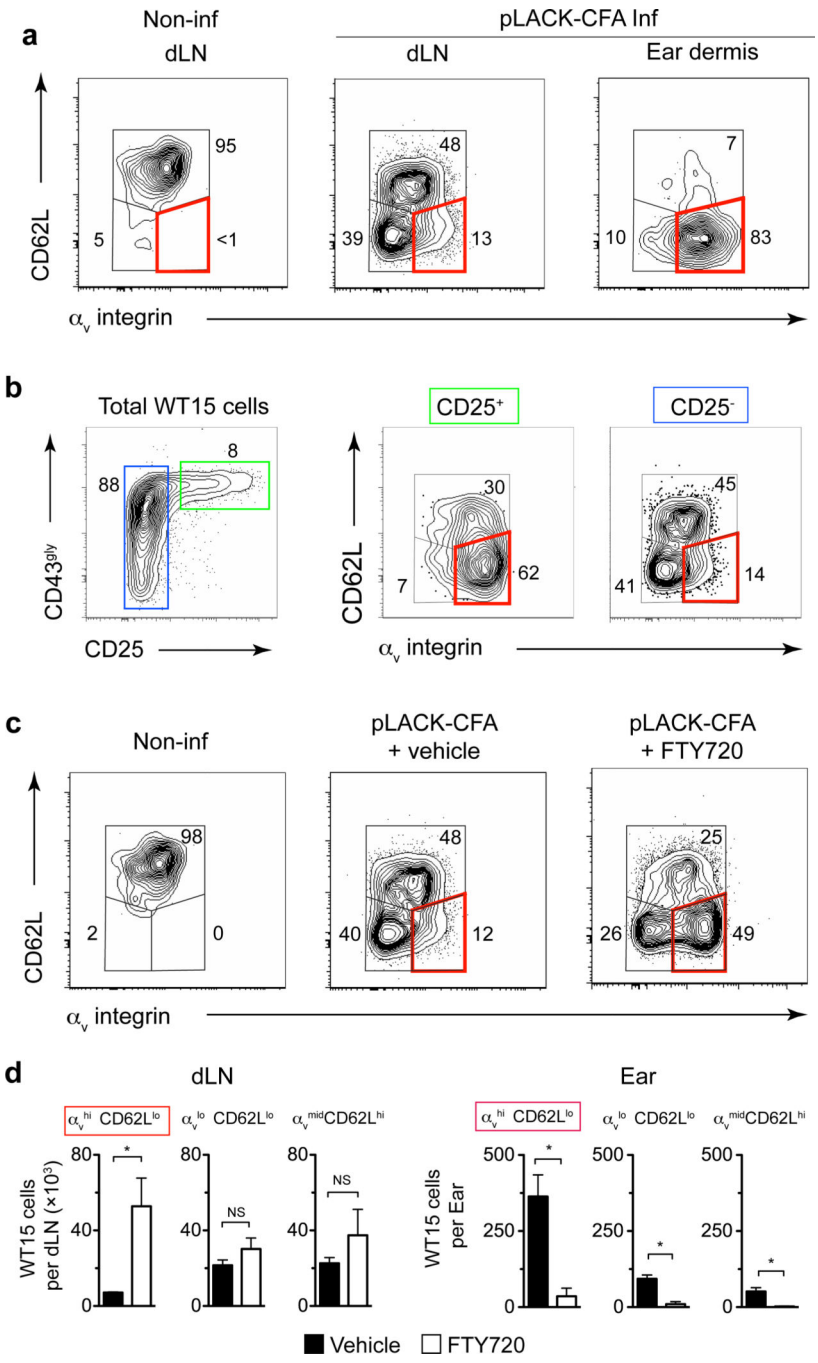

Figure 6. LN "emigrant" effector T cells express high levels of α_v integrin

Naïve WT15 cells were transferred into BALB/c mice that were then immunized with pLACK/CFA (LACK-CFA Inf) in ear dermis the following day or not immunized (Non-inf). **(a)** α_v integrin and CD62L expression on WT15 cells in the draining lymph node and ear dermis five days after immunization. Numbers represent cell frequency (%). The red box highlights the α_v^{hi} CD62L^{lo} population throughout all panels in the figure. **(b)** Expression of α_v on activated cells in the draining lymph node. Transferred cells gated on high or low expression of CD25 (left panel) and analyzed for α_v and CD62L. **(c, d)** FTY720 (or vehicle)

was administered days 3 and 4 post-immunization and α_V and CD62L expression was evaluated on WT15 cells in the lymph node on day five. **(d)** Total numbers of WT15 cells in the draining lymph node and immunized ear dermis in mice treated with FTY720 (open bars) or vehicle (filled bars). Bars represent mean ± SEM. For **(d)** statistical significance was evaluated by a Mann-Whitney test: * $p<0.05$; NS, not significant, $p>0.05$. Data are representative of two independent experiments with similar results. n= 4–5 mice per group per experiment.

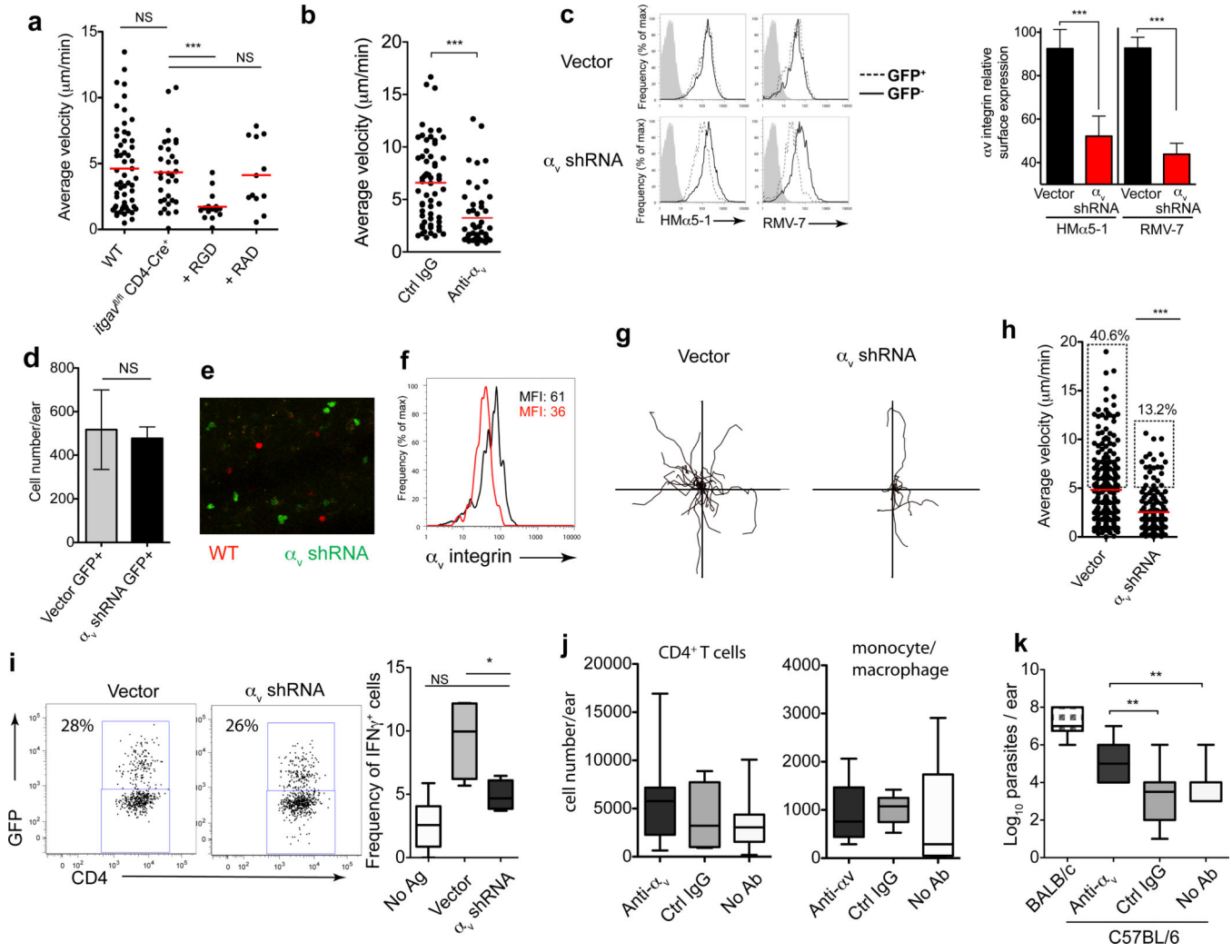

Figure 7. Non-redundant role for α_v in effector CD4$^+$ T cell intradermal motility and anti-microbial clearance

(a) α_v-deficient (*itgav*$^{fl/fl}$ × CD4-Cre+) OT-II T cell average velocity in CFA-inflamed dermis and blockade with RGD peptides as in Fig 3. **(b)** β_1-deficient OT-II T cell velocity in the CFA-inflamed ear after anti-α_v antibody. **(c)** T_H1-primed β_1-deficient OT-II T cells transduced with MSCV-GFP encoding shRNA for α_v integrin (α_v shRNA) or empty vector (Vector). Left, surface expression of α_v integrin day 4 after retroviral transduction on GFP+ and GFP- cells, with two α_v antibody clones or isotype control(grey). Right, α_v MFI of GFP + and GFP- cells, normalized to the MFI of α_v on untreated T cells. Bars represent mean ± SEM, four independent experiments. **(d–i)** Transduced T cells transferred to C57BL/6 mice and mice immunized intra-dermally with pOVA-CFA in one ear and KLH-CFA in the other ear (no cognate antigen, No Ag). Transduced T cells (GFP+) in the ear dermis imaged by IV-MPM day 3. **(d)** Number of vector or α_v shRNA GFP+ T cells in the antigen-bearing dermis. **(e)** Dermal location of effector T cells following co-injection of SNARF-labeled WT (red) and GFP+ expressing α_v shRNA (green) cells to pOVA-CFA immunized mice. **(f)** *ex vivo* α_v expression on dermal GFP+ cells. Black line, control vector; red line, α_v shRNA. **(g)** XY projections of T cell migration patterns and average velocities **(h)** (30 minutes). **(i)**

Vector control and αv shRNA GFP+ expression in pOVA-CFA inflamed ears (left). Right, frequency of IFNγ producing vector or α_v shRNA GFP+ T_H1 cells, gated as in dot plots, by *ex vivo* intracellular cytokine staining for IFN-γ. No Ag, frequency of IFN-γ^+-transferred cells in KLH-OVA inflamed ears **(j)** Mice were infected with *L. major* in the ear dermis. Four weeks post-infection, C57BL/6 mice were given anti-α_v or control antibody i.p. (1mg/mouse) three times/week for 3 weeks. Mice were harvested at week 7 post-infection and $CD4^+$ T cell numbers **(j)** and parasite load **(k)** determined in the infected ear dermis. Statistics by Mann-Whitney: *p<0.05; **p<0.01; ***p<0.001; NS, not significant, p>0.05. **(k)** ANOVA across C57BL/6 groups, p<0.0001 for parasite load.